NASA Technical Memorandum 78566

Leading-Edge Slat Optimization for Maximum Airfoil Lift

Lawrence E. Olson
Ames Research Center
Moffett Field, California

Phillip R. McGowan and Clayton J. Guest
Computer Sciences Corporation
Mountain View, California

National Aeronautics
and Space Administration

**Scientific and Technical
Information Branch**

1979

NOMENCLATURE

A wing area, cb

AR aspect ratio, b^2/A

b wing span

C_f skin friction coefficient at the upper surface trailing edge of airfoil component

C_ℓ airfoil lift coefficient, $\frac{\text{airfoil lift}}{(1/2)\rho_\infty U_\infty^2 c}$

C_L wing lift coefficient, $\frac{\text{wing lift}}{(1/2)\rho_\infty U_\infty^2 A}$

C_p airfoil surface pressure coefficient, $\frac{p - p_\infty}{(1/2)\rho_\infty U_\infty^2}$

c airfoil and wing reference chord

F $\frac{u}{u_e}$, dependent variable in boundary-layer coordinate system

L mixing length

M Mach number

p static pressure

Re reference chord Reynolds number, $\frac{U_\infty c}{\nu}$

R_θ momentum thickness Reynolds number, $\frac{U_e \theta}{\nu}$

s distance along airfoil surface, measured from stagnation point

U_∞ free-stream velocity

U_τ friction velocity, $\sqrt{\frac{\tau_w}{\rho}}$

u s-direction velocity component in boundary-layer coordinate system

V dependent variable in boundary-layer coordinate system, $(\beta - 1)F\eta + \sqrt{2\xi}\,\frac{v}{u_e}$

v y-direction velocity component in boundary-layer coordinate system

x,z airfoil coordinates

α angle of attack, deg

β pressure gradient parameter, $\left(\frac{2\xi}{U_e}\right)\frac{dU_e}{d\xi}$

δ component deflection, deg

δ^* boundary-layer displacement thickness, $\int_0^\infty \left(1 - \frac{U}{U_e}\right) dy$

ϵ eddy viscosity

η transformed boundary-layer coordinate, $\frac{U_e y}{\nu\sqrt{2\xi}}$

θ boundary-layer momentum thickness, $\int_0^\infty \frac{u}{u_e}\left(1 - \frac{u}{u_e}\right) dy$

μ molecular viscosity

ν kinematic viscosity, $\frac{\mu}{\rho}$

ξ transformed boundary-layer coordinate, $\frac{1}{\nu}\int_0^s u_e\, ds$

ρ fluid density

τ_w wall shear stress, $\mu\left(\frac{\partial u}{\partial z}\right)_{y=0}$

Subscripts:

e edge of boundary layer

f flap

i inner region of boundary layer

m main airfoil

o outer region of boundary layer

s slat

∞ free stream

LEADING-EDGE SLAT OPTIMIZATION FOR MAXIMUM AIRFOIL LIFT

Lawrence E. Olson, Phillip R. McGowan,* and Clayton J. Guest*

Ames Research Center

SUMMARY

A numerical procedure for determining the position (horizontal location, vertical location, and deflection) of a leading-edge slat that maximizes the lift of multielement airfoils is presented. The structure of the flow field is calculated by iteratively coupling potential flow and boundary-layer analysis. This aerodynamic calculation is combined with a constrained function minimization analysis to determine the position of a leading-edge slat so that the suction peak on the nose of the main airfoil is minimized. The slat position is constrained by the numerical procedure to ensure an attached boundary layer on the upper surface of the slat and to ensure negligible interaction between the slat wake and the boundary layer on the upper surface of the main airfoil. The highest angle of attack at which this optimized slat position can maintain attached flow on the main airfoil defines the optimum slat position for maximum lift. The design method is demonstrated for an airfoil equipped with a leading-edge slat and a trailing-edge, single-slotted flap. The theoretical results are compared with experimental data, obtained in the Ames 40- by 80-Foot Wind Tunnel, to verify experimentally the predicted slat position for maximum lift. The experimentally optimized slat position is in good agreement with the theoretical prediction, indicating that the theoretical procedure is a feasible design method.

1. INTRODUCTION

The multielement wing is essential for generating the high lift required of modern fixed-wing aircraft during takeoff and landing. The necessity to carry high lift results in flow fields that are strongly dependent on viscous effects. In the past, the design of these configurations has been dependent on expensive and time-consuming wind-tunnel testing to optimize the placement of the various wing elements of a high-lift system. This task is formidable because each of the three parameters (horizontal location, vertical location, and deflection) which specify the position of each flap and slat relative to the main airfoil must be optimized to yield the best aerodynamic performance. If this process could be augmented by theoretical analysis, the saving in time and wind-tunnel testing would significantly enhance the versatility and degree of optimization achievable in the development of mechanical high-lift systems.

Stevens et al. (ref. 1), Bhateley and McWhirter (ref. 2), Callaghan and Beatty (ref. 3), and Olson and Dvorak (ref. 4) present theoretical methods for the analysis of multielement airfoils. Although these analyses (all of which rely on coupled boundary-layer and potential flow analyses) differ somewhat in the methods used to determine the structure of the viscous flow, references 1 through 4 have demonstrated that, for flows in which the effects of boundary-layer separation are

*Computer Sciences Corporation, Mountain View, California 94040.

negligible, it is possible to predict the lift of multicomponent configurations with reasonable accuracy. These successes provided the impetus for utilization of these types of analysis techniques for the theoretical optimization of high-lift configurations. This optimization capability would be used to augment and, in some cases, replace experimental optimization.

The problem of designing multicomponent airfoils has been addressed by several researchers, and the following are several of the more significant examples. A design technique for shaping leading-edge slats to give a specified pressure distribution on the nose of an elliptical airfoil was developed by O'Pray (ref. 5). In his analysis, O'Pray requires that the slat position remain fixed and assumes that viscous effects are negligible. James (ref. 6) and Kennedy and Marsden (ref. 7) also present inviscid methods for generating multielement airfoils with prescribed pressure distributions, but their methods do not address the optimization problem. Ormsbee and Chen (ref. 8) have considered the shaping of a two-element airfoil so that zero turbulent skin friction is maintained in the pressure rise region on the airfoil upper surfaces. Relative movement of the two elements is permitted in the vertical direction but relative movement in the horizontal direction and deflection are not permitted.

The present paper addresses the problem of determining the *position* of a leading-edge slat so that maximum lift at stall is achieved. It is assumed that the shape of the various elements of the lifting system is known. The shapes of these elements are not modified. The theoretical method used to calculate the flow field is based on reference 4 and is outlined in Sec. II. Also described in Sec. II is the technique used to combine this viscous/potential flow aerodynamic analysis with a constrained function minimization code. Section III describes the experimental program which was conducted in the Ames 40- by 80-Foot Wind Tunnel to obtain supporting experimental data. The comparison of the theory and experiment and the concluding remarks are contained in Secs. IV and V, respectively.

II. THEORETICAL METHOD

The computerized procedure is a combination of two computer programs: (1) the aerodynamic analysis program to calculate the flow field and (2) the numerical optimization program to determine the slat position. The theoretical basis of these methods is described in the following two sections.

Aerodynamic Analysis

This analysis provides the aerodynamic information that is required as part of the design procedure. In particular, the static pressure distribution on the upper surface of the main airfoil, incipient flow separation on the slat, and incipient flow separation on the main airfoil are used in the optimization method and thus must be accurately predicted. The flow-field structure is calculated using iteratively coupled solutions of the potential flow and boundary-layer equations.

The potential flow analysis is an accurate singularity method where the airfoil contours are represented by a large number (e.g., 35 to 60 per element) of straight-line segments, on each of which is located a linear vorticity distribution. Details of this analysis are presented in reference 4.

The boundary-layer structure is calculated using the pressure field determined from the potential flow analysis. These calculations include laminar, transitional, and turbulent flows. The decision to develop a computationally efficient, finite-difference computer code for solving the boundary-layer equation was a result of the following three factors: (1) the requirement for an accurate prediction of boundary-layer displacement effects and an accurate prediction of incipient flow separation; (2) the need for an efficient computational method because the complete optimization calculation requires 500 to 2000 boundary-layer solutions to complete the slat optimization design procedure; and (3) the desire for versatility so that future studies would be possible with relatively straightforward extensions to include variation in the static pressure across the layer, turbulent wakes, and confluent turbulent boundary layers. For these reasons, a finite-difference solution to the basic equations was selected in preference to a somewhat less flexible integral approach.

Two numerical methods, the Crank-Nicolson scheme by Blottner (refs. 9 and 10) and the Keller box scheme (refs. 11 and 12) for obtaining finite-difference solutions to the boundary-layer equations were considered. Computer codes for both methods were written, and the solutions for several laminar flows were compared for speed and accuracy. The conclusions of Blottner (ref. 10) were confirmed; that is, for comparable accuracy, the Crank-Nicolson scheme is faster than the Keller box scheme by a factor of more than 3. Based on these results, the method of Blottner was selected as the most suitable for the present application. The boundary-layer equations, eddy viscosity model, laminar instability criteria, transition model, and the method by which laminar or transitional separation and reattachment is modeled are described in the appendix. A complete boundary-layer analysis takes only 0.1 to 0.2 sec on a CDC-7600 computer. A detailed description of the numerical method itself can be found in reference 10.

The structure of the confluent boundary layers, such as the wake of a wing merging with the boundary layer on a slotted flap, is determined using the finite-difference method of Dvorak and Woodward (ref. 13). The computation time required by the method of reference 1 is 20 to 30 sec on a CDC-7600 computer.

The effect of boundary-layer displacement and mass entrainment on the potential flow is simulated by distributed source panels on the airfoil contours. The strength of these source panels, as determined directly from the boundary-layer solutions, is equal to $d(U_e\delta^*)/ds$. The iteration between potential flow solutions and boundary-layer solutions is continued until convergence is achieved. Convergence was assumed to occur when the change in lift on succeeding iterations was less than 0.2%. Because the present analysis does not attempt to model the effect of flow separation, the aerodynamic analysis is limited to configurations for which the airfoil pressure distributions are not strongly affected by boundary-layer separation. This limitation has a direct effect on the method used to determine the optimum slat location.

Optimization Method

The objective of the optimization procedure is to find the slat location and deflection required for maximum lift. To achieve this goal without actually performing aerodynamic calculations for flows with massive amounts of flow separation, a method has been developed which is based on the analysis of configurations that are constrained so that attached flow is maintained. The fundamental assumption made in the analysis is that the optimum slat position for maximum lift is closely approximated by the slat position that minimizes the suction peak on the upper surface of the main

element. This optimum slat position is determined at the highest angle of attack at which attached flow can be maintained on the upper surface of the main element. An alternative view of the analysis is that the nearly linear portion of the C_ℓ versus α curve is being extended to as high a lift coefficient as possible by proper placement of the leading-edge slat. It is assumed that maximizing the lift coefficient at which flow separation first occurs will also maximize $C_{\ell_{max}}$. For configurations that stall abruptly, this is a reasonable premise; however, for airfoils that stall gradually, the validity of this assumption is questionable. The validity of the method is tested, for a configuration with abrupt stalling characteristics, by comparison of theoretical predictions with experimental measurements.

The constrained function minimization method described in detail by Vanderplaats (ref. 14) and by Vanderplaats and Moses (ref. 15) is used in combination with the aerodynamic analysis described in the previous section to optimize the slat position. An example of the application of this analysis to inviscid single-element airfoil design for minimum wave drag at transonic speeds is presented by Hicks et al. (ref. 16). In the present analysis, the function to be minimized is the suction peak on the upper surface of the main element. This minimization is performed with the main airfoil element at a fixed angle of attack. The design variables are slat horizontal position, slat vertical location, and slat deflection. For the three element airfoil considered in this report (see fig. 1), the slat horizontal and vertical locations are defined by the position of the slat trailing edge. The pivot point of the slat is located at the slat trailing edge. Thus, all three parameters can be varied independently.

Slat translation and deflection are subject to two constraints. The first constraint is that there be no flow separation on the slat upper surface. This prevents the aerodynamic program from attempting calculations in the separated flow regime. Mathematically, this constraint is $C_{f_S} > 0.0001$, where C_{f_S} is the skin friction coefficient at the trailing edge of the upper surface of the slat. The second constraint requires that the trailing edge of the slat does not get closer than 0.02 c to the upper surface of the main element. This prevents the viscous wake of the slat from merging with the boundary layer on the wing upper surface. The validity of this constraint is supported by the experimental work of Lungstrom (ref. 17) where it is shown that the optimum slat gap occurs when the wake of the slat does not interact strongly with the boundary layer on the wing. Since the constraint prevents the merging of the slat wake and the boundary layer on the upper surface of the wing, the computationally time-consuming, confluent boundary-layer calculation is replaced by a computationally efficient, conventional boundary-layer calculation. This constraint is expressed as $G > 0.02$ c, where G is the distance between the trailing edge of the flap and the surface of the main airfoil.

The confluent boundary layer on the upper surface of the flap is analyzed with the slat in its initial position. Thereafter, the displacement effect of the confluent boundary layer of the flap is held fixed during the numerical search for the slat position that minimizes the suction peak on the main airfoil. After the slat position is determined, the confluent boundary layer is then recomputed to ensure that the displacement effect is not substantially different from that with the initial slat position.

Theoretical Results

Figure 2 shows a sequence of positions through which the slat moved during the numerical design procedure. For this particular example, the angle of attack of the main airfoil is 15°. With the slat in the initial position (slat position No. 1) the slat is lightly loaded, whereas the leading-edge region of the main airfoil is highly loaded resulting in a large suction peak and a strong adverse pressure gradient. After nine iterations, each requiring the calculation of the gradient of the suction peak with respect to three slat position variables, and for most iterations the calculation of the gradient of one or both of the constraints as well, the analysis has converged and the slat position that minimizes the suction peak on the main airfoil has been determined. In this final position, the suction peak, and therefore the adverse pressure gradient on the main airfoil, has been substantially reduced in exchange for an increased loading on the slat. The numerical design yields a slat loading that is limited only by the constraint that flow separation not occur on the slat upper surface. Figure 3 shows the surface pressure distributions for angles of attack of the main airfoil of 13°, 19°, and 24°. At each of these angles of attack, the slat position is such that the suction peak is minimized and the boundary layer on the upper surface of the slat is on the verge of separation.

Figure 4 shows the variation in slat horizontal position, slat vertical position, and slat deflection for angles of attack ranging from 13° to 24°. Also shown is the skin-friction coefficient at the trailing edge of the upper surface of the main element. Note that as the angle of attack is increased, the boundary layer on the main airfoil approaches separation ($C_{f_m} \rightarrow 0$) due to an increase in the adverse pressure gradient (Fig. 3) – even though the slat is maintained in a position that minimizes the suction peak in the leading-edge region. Extrapolation of these numerical results predicts incipient flow separation ($C_{f_m} = 0$) on the main airfoil at an angle of attack of 25°. The slat position for this angle of attack is specified as the theoretically predicted optimum location required to give maximum lift. This assumption will be verified by comparison with experiment.

III. WIND-TUNNEL TEST PROGRAM

As part of this study, wind-tunnel tests were conducted in the Ames 40- by 80-Foot Wind Tunnel to verify the reliability of the theoretical predictions by experimentally determining the optimum position of the leading-edge slat.

A rectangular planform wing was used in these tests (fig. 5). The wing was equipped with a full-span leading-edge slat and a full-span single-slotted flap. The slat chord was 0.17 c and the flap chord was 0.40 c. A detailed description of the slat, main airfoil, and flap shapes is given in reference 16. The wing span is 16 m and the extended chord is 2.15 m. The relatively high aspect ratio of 7.5, combined with the rectangular planform, resulted in a configuration with nearly two-dimensional flow over much of the wing span. Also, the use of a high aspect ratio finite wing eliminated adverse wind-tunnel wall interference effects associated with two-dimensional, high-lift airfoils which span the entire test section.

The slat brackets permitted continuous adjustment of horizontal location, slat vertical location, and slat deflection. The range of movement in the horizontal and vertical directions was 0.04 c and 0.05 c, respectively. The forces and moments on the wing were measured along the model centerline for a limited number of test conditions. All data were obtained at a Reynolds

number of 3.8×10^6 and a Mach number of 0.10. The flap location and deflection angle ($\delta_f = 10°$) were held fixed throughout the test. The gap between the trailing edge of the wing and the upper surface of the flap was 0.03 c and the flap leading edge was located at 0.04 c ahead of the trailing edge of the main airfoil. This flap position is representative of a takeoff flap setting.

As was discussed in Sec. II, the aerodynamic calculations are based on a method that does not model extensive flow-separation effects. Thus, it is expected that this type of analysis will be most accurate when the configuration being considered has an abrupt, rather than gradual, stall. The measured lift curve for this wing is shown in figure 6. It is nearly linear up to an angle of attack of 26°. At an angle of attack of 26°, the wing abruptly stalls. Thus, flow-separation effects are expected to be negligible at angles of attack below stall. Figure 7 shows a comparison of the theoretically computed and the measured airfoil section pressure distribution at a lift coefficient just below stall. The experimental data are for a wing angle of attack of 24°. The center-section loading corresponds to a section angle of attack of 20° and a section C_ℓ of 3.1. These results verify that the aerodynamic analysis method is able to accurately predict the upper surface pressure distributions, even when flow separation is incipient. This is essential to the design procedure because at the final design condition, both the boundary layer on the upper surface of the slat and the boundary layer on the upper surface of the wing are on the verge of separating.

IV. COMPARISON OF THEORY AND EXPERIMENT

The experimental optimization data are summarized in figures 8–10. The variation of $C_{L_{max}}$ with horizontal position of the slat, vertical position of the slat, and deflection of the slat is shown. Also shown on the figures are the theoretically optimized trailing-edge position of the slat and the slat deflection. The predicted horizontal and vertical locations of the slat are within 0.003 c and 0.007 c, respectively, of the experimental value. The theoretically determined slat deflection is −36°, whereas the experimental value is −40°. The net result is that the theoretically optimized slat position is 4° nose up and 0.008 c aft and up relative to the experimentally optimized location.

Figure 11 shows the theoretically and experimentally optimized slat positions relative to the leading edge of the main element. With the slat in the theoretically optimized location, the measured maximum lift coefficient of the wing is 3.16 and with the slat in the experimentally optimized location, the measured maximum lift coefficient of the wings is 3.28, a difference of only 4%.

The most significant difference between the predicted and measured optimum positions is the 4° in deflection. The theoretical results indicate that the slat can sustain a greater loading than was found experimentally. Although it is not possible to determine precisely why this occurs, inaccuracy in the prediction of incipient flow separation of the boundary layer on the upper surface of the slat is probably the cause because this separation has a direct influence on the optimized slat deflection.

The relatively good agreement between theory and experiment shows that the theoretical optimization technique is useful for estimating the position of leading-edge slats that results in maximum lift. Using the theoretical predictions as starting conditions, the wind-tunnel testing required to experimentally optimize multielement airfoils can be significantly reduced.

V. CONCLUDING REMARKS

A design method for the optimization of the position of a leading-edge slat so that maximum airfoil lift is obtained has been successfully demonstrated. For an airfoil equipped with a leading-edge slat and a single-slotted flap, the measured maximum lift with the slat in the theoretically determined optimum position is within 4% of the measured maximum lift with the slat in the experimentally optimized position. The analysis is limited to configurations that do not have significant flow separation at angles of attack below stall. The details of the flow-field structure are modeled, using iteratively coupled potential flow and boundary-layer analysis. Accurate prediction of incipient flow separation of the upper surface boundary layers on the slat and on the main wing provide the viscous constraints which are essential to the design procedure. It is concluded that, for multielement airfoils that do not have extensive flow-separation effects at angles of attack near stall and thus have relatively abrupt stalling characteristics, minimization of the suction peak on the main component combined with incipient flow separation on both the slat and main component is a valid method for optimizing the position of a leading-edge slat for maximum lift.

Ames Research Center
National Aeronautics and Space Administration
Moffett Field, California 94035, March 22, 1979

APPENDIX

ANALYSIS OF VISCOUS FLOW

The Levy-Lees form of the incompressible turbulent boundary-layer equations is:

$$2\xi \frac{\partial F}{\partial \xi} + \frac{\partial V}{\partial \eta} + F = 0 \tag{A2}$$

$$2\xi F \frac{\partial F}{\partial \xi} + V \frac{\partial F}{\partial \eta} - \beta(1 - F^2) - \frac{\partial}{\partial \eta}\left(\ell \frac{\partial F}{\partial \eta}\right) = 0 \tag{A2}$$

where

$$F = \frac{U}{U_e}, \quad V = (\beta - 1)F\eta + \sqrt{2\xi}\frac{v}{U_e}, \quad \beta = \frac{2\xi}{U_e}\frac{dU_e}{d\xi} \tag{A3}$$

$$\eta = \frac{U_e}{\nu\sqrt{2\xi}} y, \quad \xi = \frac{1}{\nu}\int_0^s U_e\, ds \tag{A4}$$

The coefficient ℓ is defined as,

$$\ell = 1 + \frac{\epsilon}{\nu} \tag{A5}$$

where ϵ is the eddy viscosity. An eddy viscosity model which combines the recommendation of Cebeci (ref. 18) and Cebeci et al. (ref. 19) is used to calculate the Reynolds stresses for the transitional and turbulent boundary layers. In the inner region of the boundary layer, the eddy viscosity is denoted by ϵ_i; in the outer region it is denoted by ϵ_o. When these parameters are reduced to their incompressible form and the effects of mass transfer are neglected:

$$\epsilon_i = L^2\left|\frac{\partial u}{\partial y}\right|\gamma_{tr} \tag{A6}$$

and

$$\epsilon_o = \alpha u_e \delta^* \gamma_{tr} \tag{A7}$$

where L, the mixing length for the inner region, is given by

$$L = ky\left[1 - \exp\left(\frac{y}{A}\right)\right] \tag{A8}$$

and

$$k = 0.40 + \frac{0.19}{1 + 0.49\times10^{-6}R_\theta^2} \tag{A9}$$

$$A = \frac{\nu}{NU_\tau^{1/2}}\left(26 + \frac{14}{1 + 10^{-6}R_\theta^2}\right) \tag{A10}$$

$$N = 1 - 11.8\,\frac{\nu u_e}{u_\tau^3}\,\frac{du_e}{ds} \tag{A11}$$

$$U_\tau = \left[\frac{\tau_w}{\rho}\right]^{1/2} \tag{A12}$$

A parameter γ_{tr} is introduced to control the overall Reynolds stress level during transition. At the point of laminar instability, $\gamma_{tr} = 0$, and for fully turbulent flow, $\gamma_{tr} = 1$. In the transition zone

$$\gamma_{tr} = 1 - \exp\left(-(s - s_{tr})G\int_{s_{tr}}^{s}\frac{ds}{u_e}\right) \tag{A13}$$

where

$$G = \frac{U_e^3}{\nu^2}\,\frac{R_{\theta_{tr}}^{-2.68}}{B}\quad,\quad B = 60 + 4.68M_e^{1.63} \tag{A14}$$

s_{tr} and $R_{\theta_{tr}}$ are evaluated at the point of laminar instability.

The correlations of Smith (ref. 20) are used to determine the location of laminar instability. These equations are

$$K_{tr} = -0.4709 + 0.11066\ln R_\theta - 0.005891(\ln R_\theta)^2 \tag{A15}$$

for $R_\theta \leqslant 650$, and

$$K_{tr} = 0.69412 - 0.23992\ln R_\theta + 0.0205(\ln R_\theta)^2 \tag{A16}$$

for $R_\theta > 650$

where

$$\frac{\zeta^2}{\nu}\,\frac{dU_e}{ds} \leqslant K_{tr} \tag{A17}$$

indicates laminar instability.

If laminar or transitional boundary-layer separation occurs, the correlation of Gastor (ref. 21) is used to determine if turbulent reattachment occurs. These equations are

$$K_{sep} = -0.09 \tag{A18}$$

for $R_\theta < 125$, and

$$K_{sep} = 0.027 - 0.7575 \times 10^{-3} R_\theta - 1.157 \times 10^{-6} R_\theta^2 \tag{A19}$$

for $R_\theta \geq 125$ where turbulent reattachment is indicated when

$$\frac{\theta^2}{\nu} \frac{dU_e}{ds} \leq K_{sep} \tag{A20}$$

If catastrophic separation is indicated, the boundary-layer calculation is terminated. If laminar separation followed by turbulent reattachment is indicated, then transition to turbulent flow is initiated at the separation point. Should transitional boundary-layer separation occur, the local adverse pressure gradient is reduced until an attached flow solution of the boundary-layer equations is obtained. In this case, a nearly zero skin-friction solution is obtained for the transitional reattaching boundary layer.

1. Stevens, W. A.; Goradia, S. H.; and Branden, J. A.: Mathematical Model for Two-Dimensional Multi-Component Airfoils in Viscous Flow. NASA CR-1843, July 1971.

2. Bhateley, Ishwar C.; and McWhirter, Jack W.: Development of Theoretical Methods for Two-Dimensional Multi-Element Airfoil Analysis and Design. Part I: Viscous-Flow Analysis Method. AFFDL-TR-72-96, Part I, Aug. 1972.

3. Callaghan, J. G.; and Beatty, T. V.: A Theoretical Method for the Analysis and Design of Multielement Airfoils. J. Aircraft, vol. 9, no. 12, Dec. 1972, pp. 844–848.

4. Olson, L. E.; and Dvorak, F. A.: Viscous/Potential Flow about Multi-Element Two-Dimensional and Infinite-Span Swept Wings: Theory and Experiment. AIAA Paper 76-18, AIAA 14th Aerosp. Sci. Mtg., Wash., D.C., Jan. 26–28, 1976.

5. O'Pray, John Edwin: A Semi-Inverse Design Technique for Leading-Edge Slats. Ph.D. Thesis, Calif. Inst. of Tech., Pasadena, Calif., May 1970.

6. James, R. M.: The Theory and Design of Two-Airfoil Lifting Systems. Computer Methods in Appl. Mech. and Eng., vol. 10, no. 1, 1977, pp. 13–43.

7. Kennedy, J. L.; and Marsden, D. J.: A Potential Flow Design Method for Multicomponent Airfoil Sections. J. Aircraft, vol. 15, no. 1, Jan. 1978, pp. 47–52.

8. Ormsbee, Allen I.; and Chen, Allen W.: Multiple Element Airfoils Optimized for Maximum Lift Coefficient. AIAA J., vol. 10, no. 12, Dec. 1972, pp. 1620–1624.

9. Blottner, F. G.: Variable Grid Scheme Applied to Turbulent Boundary Layers. Computer Methods in Appl. Mech. and Eng., vol. 4, no. 2, Sept. 1974, pp. 179–194.

10. Blottner, F. G.: Investigation of Some Finite-Difference Techniques for Solving the Boundary Layer Equations. Computer Methods in Appl. Mech. and Eng., vol. 6, no. 1, July 1975, pp. 1–30.

11. Keller, H. B.: A New Difference Scheme for Parabolic Problems. Numerical Solution of Partial Differential Equations 2, J. Brable, ed., Academic Press, New York, 1971, pp. 327–350.

12. Keller, Herbert B.: Accurate Difference Methods for Nonlinear Two-Point Boundary Value Problems. SIAM J. Numerical Analysis, vol. 11, no. 2, April 1974, pp. 305–320.

13. Dvorak, F. A.; and Woodward, F. A.: A Viscous/Potential Flow Interaction Analysis Method for Multi-Element Infinite Swept Wings, vol. 1, NASA CR-2476, Nov. 1974.

14. Vanderplaats, Garrett N.: COMIN – A Fortran Program for Constrained Function Minimizations: User's Manual. NASA TM X-62,282, Aug. 1973.

15. Vanderplaats, Garrett N.; and Moses, Fred: Structural Optimization by Methods of Feasible Directions. Computers and Structures, vol. 3, July 1973, pp. 739–755.

16. Hicks, Raymond M.; Murman, Farll M.; and Vanderplaats, Garret N.: An Assessment of Airfoil Design by Numerical Optimization. NASA TM X-3092, July 1974.

17. Ljungstrom, Bjorn, L. G.: 2-D Wind-Tunnel Experiments with Double and Triple Slotted Flaps. Aeronautical Research Institute of Sweden, FFA-TN AU-993, Nov. 1973.

18. Cebeci, Tuncer: Calculation of Three-Dimensional Boundary Layers I. Swept Infinite Cylinders and Small Cross Flow. AIAA J., vol. 12, no. 6, June 1974, pp. 779–786.

19. Cebeci, T.; Kaups, K.; Mosinskis, G. J.; and Rehn, J. A.: Some Problems of Calculation of Three-Dimensional Boundary-Layer Flows on General Configurations. NASA CR-2285, July 1973.

20. Smith, A. M. O.: Transition, Pressure Gradient, and Stability Theory. Proc. 9th International Congress of Applied Mechanics, Brussels, vol. 7, 1957, pp. 234–244.

21. Gaster, M.: The Structure and Behavior of Laminar Separation Bubbles. ARC 28-226, 1969, revised.

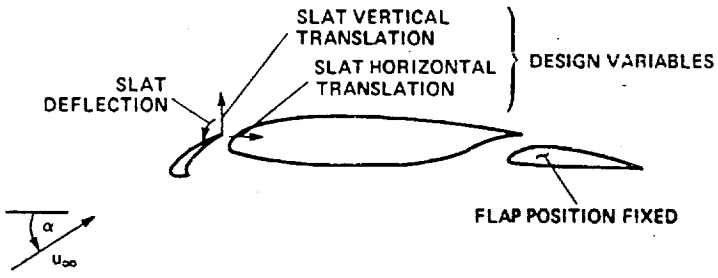

Figure 1.– Three-element airfoil used in the investigation: $\delta_f = 10°$.

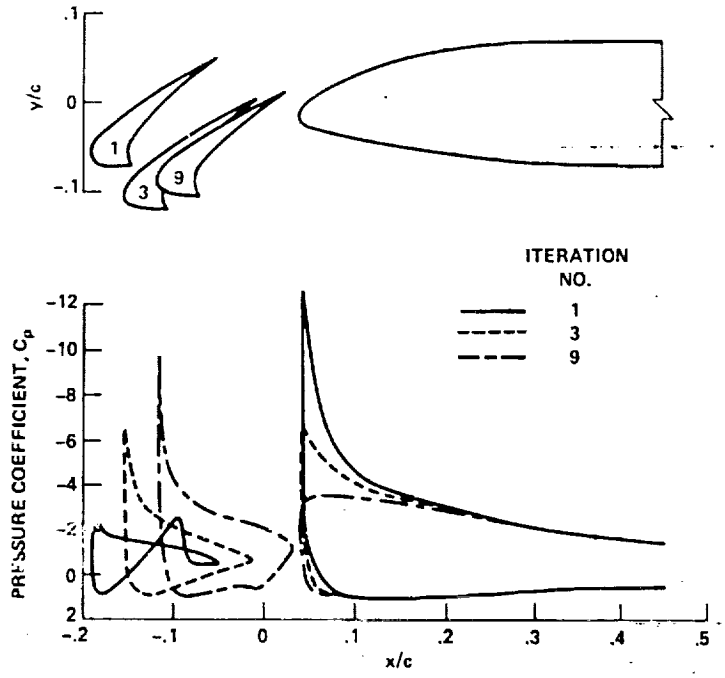

Figure 2.– Minimization of suction peak on main airfoil at an angle of attack of 15°: $\delta_f = 10°$, $Re = 3.8 \times 10^6$.

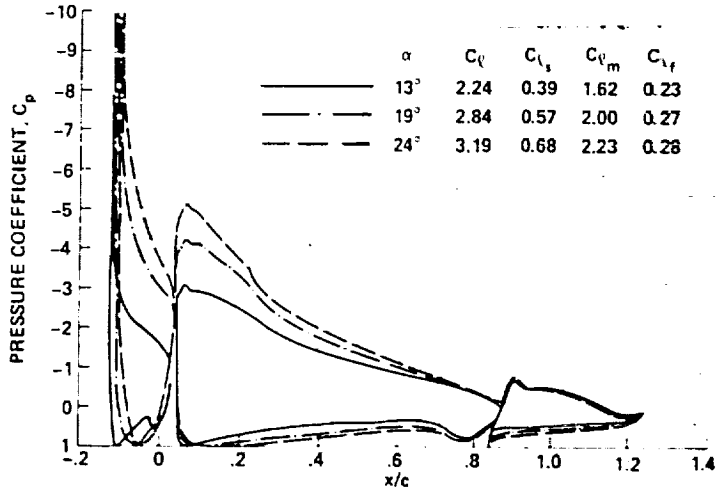

Figure 3.– Airfoil pressure distributions with slat positioned to minimize the suction peak on main airfoil: $\delta_f = 10°$, $Re = 3.8 \times 10^6$.

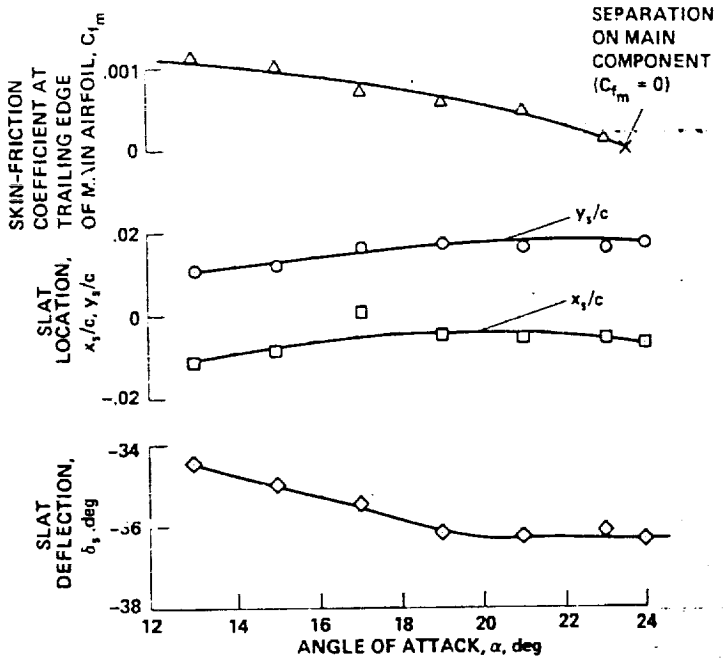

Figure 4.– Effect of angle of attack on slat position required to minimize suction peak and the corresponding skin friction coefficient at the trailing edge of the main airfoil: $\delta_f = 10°$, $Re = 3.8 \times 10^6$.

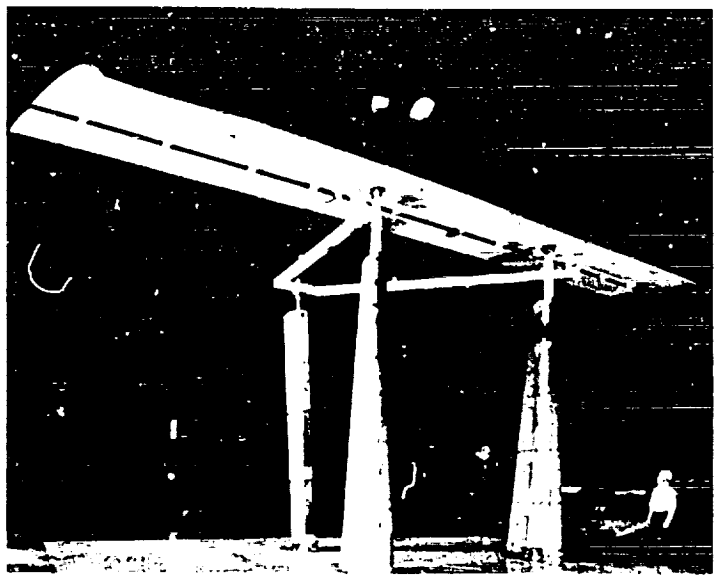

Figure 5.– Wind-tunnel model used to experimentally determine optimum slat position required for maximum lift.

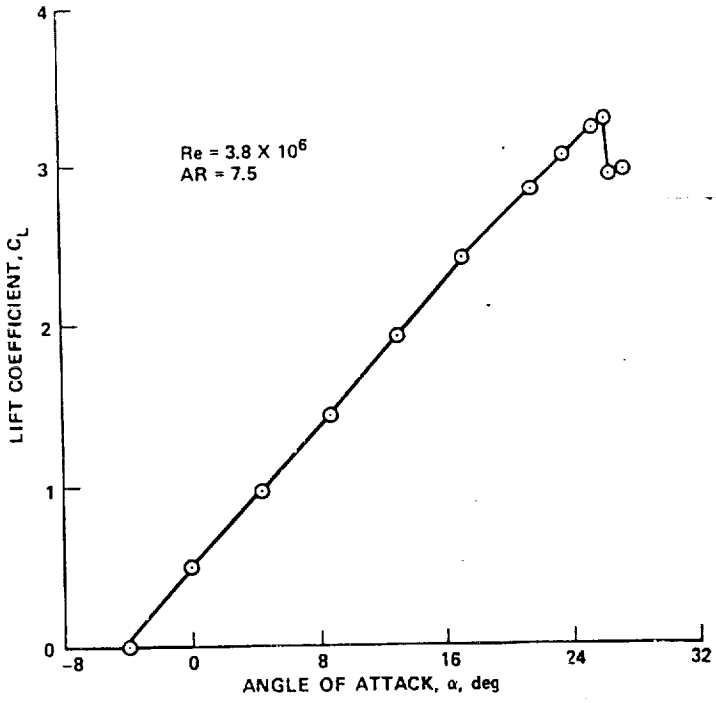

Figure 6.– Wing lift coefficient as a function of angle of attack showing nearly linear lift curve and abrupt stall: $\delta_s = -40°$, $x_s/c = -0.01$, $y_s/c = 0.01$, $\delta_f = 10°$, $Re = 3.8 \times 10^6$.

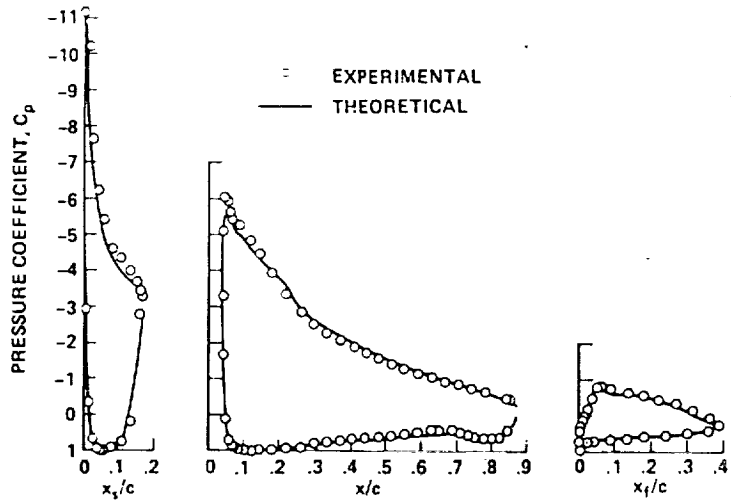

Figure 7.– Comparison of theoretical and experimental pressure distributions near stall with a section lift coefficient of 3.1: $\delta_S = -42°$, $x_S/c = -0.01$, $y_S/c = 0.02$, $\delta_S = 10°$, $Re = 3.8 \times 10^6$.

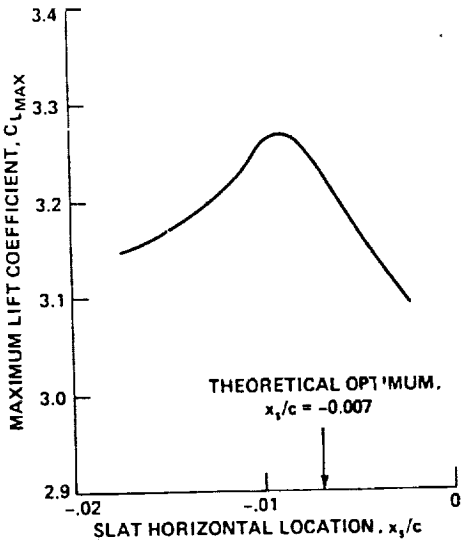

Figure 8.– Effect of slat trailing-edge horizontal location on wing maximum lift: $\delta_s = -40°$, $y_s/c = 0.01$, $\delta_f = 10°$, $Re = 3.8 \times 10^6$.

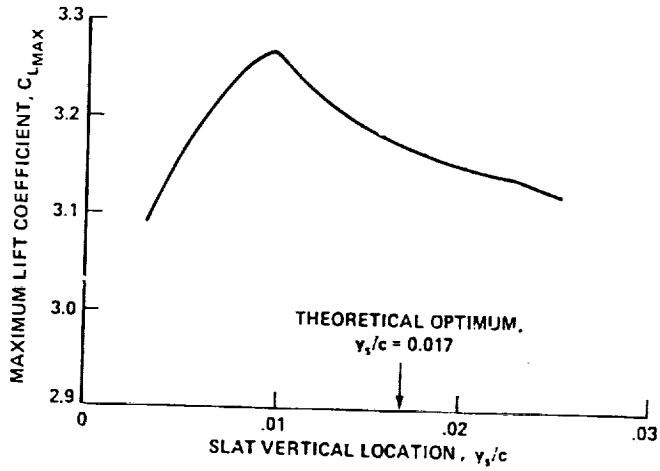

Figure 9.– Effect of slat trailing-edge vertical location on wing maximum lift: $\delta_s = -40°$, $x_s/c = -0.09$, $\delta_f = 10°$, $Rc = 3.8 \times 10^6$.

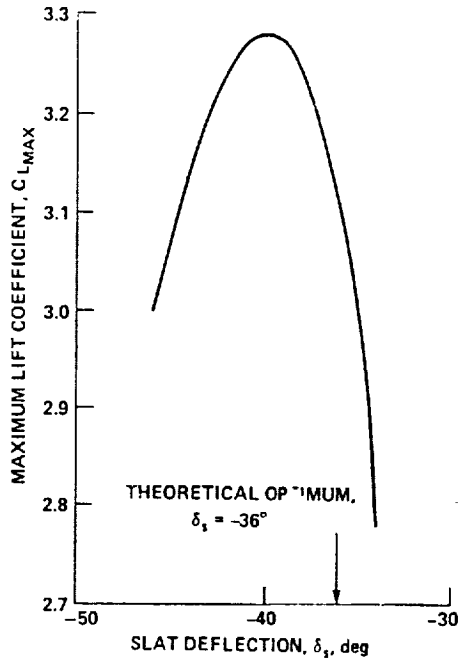

Figure 10.– Effect of slat deflection on wing maximum lift: $x_s/c = -0.09$, $y_s/c = 0.01$, $\delta_f = 10°$, $Re = 3.8 \times 10^6$.

SLAT LOCATION	x_s/c	y_s/c	δ_s	$C_{L_{MAX}}$(EXPERIMENTAL)
A	-0.007	0.017	-36°	3.16
B	-0.009	0.010	-40°	3.28

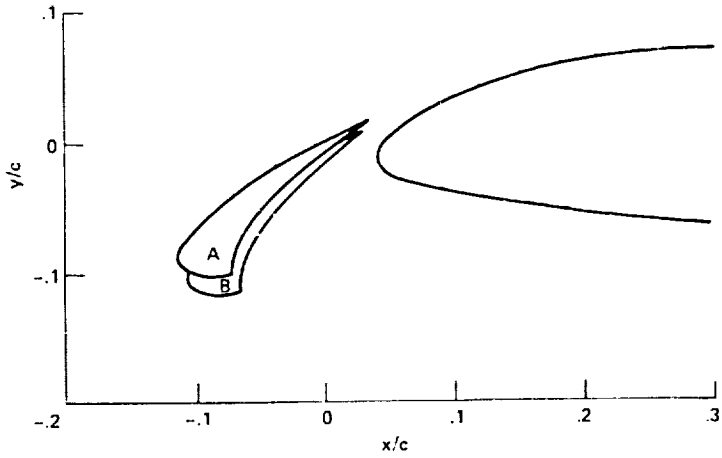

Figure 11.– Comparison of theoretically optimized and experimentally optimized slat positions: position A = theoretical, position B = experimental, $\delta_f = 10°$, $Re = 3.8 \times 10^6$.